Heat Transfer and Pressure Drop Characteristics of Finned Metal Foam Heat Sinks Under Uniform Impinging Flow

Article *in* Journal of Electronic Packaging · June 2015

DOI: 10.1115/1.4029722

CITATIONS
2

READS
88

4 authors, including:

Shangsheng Feng
Xi'an Jiaotong University
39 PUBLICATIONS **109** CITATIONS
SEE PROFILE

Tian Jian Lu
Xi'an Jiaotong University
551 PUBLICATIONS **8,635** CITATIONS
SEE PROFILE

S. S. Feng
MOE Key Laboratory for Multifunctional Materials and Structures (LMMS);
State Key Laboratory of Mechanical Structure Strength and Vibration,
Xi'an Jiaotong University,
Xi'an, Shaanxi, 710049, China

J. J. Kuang
MOE Key Laboratory for Multifunctional Materials and Structures (LMMS);
School of Energy and Power Engineering,
Xi'an Jiaotong University,
Xi'an, Shaanxi, 710049, China

T. J. Lu[1]
MOE Key Laboratory for Multifunctional Materials and Structures (LMMS);
State Key Laboratory of Mechanical Structure Strength and Vibration,
Xi'an Jiaotong University,
Xi'an, Shaanxi, 710049, China
e-mail: tjlu@mail.xjtu.edu.cn

K. Ichimiya
Department of Mechanical Engineering,
University of Yamanashi,
4-3-11 Kofu,
Yamanashi 400-8511, Japan

Heat Transfer and Pressure Drop Characteristics of Finned Metal Foam Heat Sinks Under Uniform Impinging Flow

A numerical investigation was carried out to characterize the thermal performance of finned metal foam heat sinks subject to an impinging air flow. The main objective of the study was to quantify the effects of all relevant configurational parameters (channel length, channel width, fin thickness, and fin height) of the heat sink upon the thermal performance. Open-cell aluminum foam having fixed porosity of 0.9118 and fixed pore density of five pores per inch (PPI) was used in the study. A previously validated model based on the porous medium approach was employed for the numerical simulation. Various simulation cases for different combinations of channel parameters were carried out to obtain the Nusselt number correlation. Based on the inviscid impinging flow, a pressure drop correlation was derived for impinging flow in finned metal foam heat sinks. By using these correlations, the thermal performance of finned metal foam heat sinks was compared with the conventional plate-fin heat sinks. It was demonstrated that the finned metal foam heat sinks outperformed the plate-fin heat sinks on the basis of given weight or given pumping power. [DOI: 10.1115/1.4029722]

Keywords: metal foam, finned metal foam, impinging jet, electronic cooling

1 Introduction

With the advent of modern electronic computers, cooling electronic chips have become one of the principal subjects for heat transfer science and engineering [1]. Although various advanced cooling systems have been suggested (e.g., thermoelectric cooling, liquid cooling, two-phase cooling, etc.) [2–4], the solution with air-cooled heat sinks is preferred because of its reliability and cost-effectiveness [5]. To enhance the rate of heat dissipation from an air-cooled heat sink, the simple approach is to increase heat sink size or the air flow rate. However, the spacing for housing the heat sink is often limited in electronic devices, and the air flow rate is also limited by the maximum allowable acoustic noise and fan power consumption. Therefore, the main design concern is to find the best heat transfer medium (or heat sink) which can maximize the heat dissipation with the volume of heat sink and operating condition of the cooling fan fixed. The heat dissipation of a heat transfer medium is a complex function of many factors, e.g., available heat transfer area, heat conduction, interstitial heat transfer coefficient, and flow resistance characteristics. These factors are strongly dependent on the structure of a heat transfer medium; and they conflict with each other, for example, higher surface area and stronger heat conduction capability usually lead to larger flow resistance. A good heat transfer medium should well balance these conflicting factors. In this regard, finding the "best" heat transfer medium with novel structure and material is a perpetual pursuit to satisfy the ever-increasing heat transfer demands in the electronics industry.

As the most common heat transfer medium, plate-fin heat sinks have been extensively studied subject to impinging air flow. Biber [6] numerically studied an isothermal channel with a number of different combinations of channel parameters and presented correlations of pressure loss coefficient and Nusselt number for plate-fin heat sinks. Saini and Webb [7] compared their experimental data for plate-fin heat sinks with predictions obtained with the Biber model and found that the Biber model underpredicted the measured pressure drop by about 13–31% and overpredicted the heat transfer data by approximately 11%. Based on developing laminar flow in rectangular channels, Duan and Muzychka [8,9] developed simple models for Nusselt number and pressure drop of plate-fin heat sinks. Kondo et al. [10] used a semi-empirical zonal model to optimize the parameters of plate-fin heat sinks under given operating condition of cooling fan. Kim et al. [11–13] developed a porous medium model for plate- and pin-fin heat sinks subject to uniform impinging air jet. Particularly, based on the assumptions of isothermal fins and inviscid impinging flow in finned heat sinks, simple closed form expressions were obtained for pressure drop and thermal resistance [11].

Another popular cooling technique is heat transfer augmentation using porous medium [14]. High porosity open-cell metal foams are of great interest for heat transfer augmentation [15–19], since they can attain a high heat transfer rate but associated with much lower pressure drop than other porous medium such as packed bed. Kuo and Tien [15] presented one of the pioneer works utilizing open-cell foams to enhance liquid forced convection for electronic cooling. Recently, enhanced cooling technique using open-cell metal foams combined with impinging jet has drawn much attention due to its great potential for high heat flux removal applications including electronics cooling. Jeng and Tzeng [20] numerically investigated the effects of foam height and Reynolds number on the heat transfer performance of an aluminum foam heat sink subject to confined slot impinging air jet. Ejlali et al.

[1]Corresponding author.

Contributed by the Electronic and Photonic Packaging Division of ASME for publication in the JOURNAL OF ELECTRONIC PACKAGING. Manuscript received November 22, 2013; final manuscript received January 28, 2015; published online February 20, 2015. Assoc. Editor: Pradip Dutta.

[21] numerically studied and found that the thermal performance of an impinging air cooled metal foam heat exchanger was superior to conventional finned surfaces at no excess cost (material weight and/or pressure drop). Based on the local thermal equilibrium assumption, Vafai and coworkers [22] numerically investigated the mixed convection heat transfer behavior of a metal foam heat sink under a confined slot impinging jet. Focusing on electronic cooling, Kuang et al. [23] experimentally examined the performance of metal foam heat sinks subject to axial fan flow impingement. Shih et al. [24] performed experiments on aluminum foam heat sinks having different heights and found the existence of optimal foam height for maximum heat dissipation. Targeting turbine cooling, Rallabandi et al. [25] measured under air jet impingement conditions the heat transfer and pressure drop characteristics of a high aspect ratio duct with three types of roughness element: staggered axial ribs, inline axial ribs, and aluminum foam. It was demonstrated that the foam provided a significantly higher heat transfer coefficient than the conventional rib roughness elements.

By sandwiching metal foam blocks between the fins within a plate-fin heat sink, Bhattacharya and Mahajan [26,27] proposed a new type of heat sink, named as "finned metal foam heat sink." They experimentally tested and found that finned metal foam heat sinks outperformed metal foam heat sinks by a factor between 1.5 and 2 in both forced convection and natural convection. Later, DeGroot et al. [28] developed a numerical model for heat transfer of finned metal foam heat sinks under parallel forced convection and carried out case studies according to the experimental conditions in Ref. [26]. Recently, using three-dimensional printing and investment casting techniques, Krishnan et al. [29] fabricated and studied finned metal foam heat sinks with regular foam structures, they concluded that on an equal pumping power basis, finned metal foam heat sinks outperformed conventional plate-fin heat sinks. Above studies demonstrate the importance of finned metal foam heat sinks for heat transfer enhancement.

On the other hand, all of the aforementioned studies investigated the thermal performance of finned metal foam heat sinks under parallel forced convection, few studies concerned the impinging cooling characteristics of finned metal foam heat sinks. Impinging cooling has been widely used in the electronics cooling industry due to its advantages over parallel forced convection. For example, impinging cooling requires no flow guiding channels around the heat sink and is easier to implement. Second, compared to parallel flow, it retains lower pressure drop and smaller temperature difference of the cooling flow within the heat sink [12].

Feng et al. [30] have built a numerical model based on the porous medium approach for finned metal foam heat sinks subject to impinging air cooling and experimentally validated the model for both the heat transfer and pressure drop. The authors found that the numerical model can accurately predict both the heat transfer and pressure drop of finned metal foam heat sinks if the foam properties were exact. However, influence of various design parameters (e.g., length and height of heat sink, fin distance, and fin thickness) on the thermal performance was not systematically investigated in Ref. [30]. The objective of the present study was to quantify the effects of these parameters using our previously validated numerical model in Ref. [30]. While the foam properties (e.g., pore size and porosity) were not variables, an electroretinographic (ERG Duocel®, ERG Materials and Aerospace Corp., Oakland, CA) aluminum foam tested in Ref. [31] was fixed in the study, which had a pore size of 5 PPI and a porosity of 0.9118. The rationale behind selecting this particular foam (5 PPI, 0.9118 porosity) is that, under a given pressure drop, a foam having a relatively large pore size and low porosity yields better heat transfer performance in either forced convection [26] or natural convection [27]. Since the limits for pore size and porosity of the commercially available ERG foams are around 5 PPI and 0.9, respectively, using the present foam of 5 PPI and 0.9118 porosity may therefore be representative for achieving the best heat transfer performance. With the foam properties fixed, a number of simulation cases were carried out for different combinations of variables to obtain the Nusselt number correlation. Based on inviscid impinging flow assumption, a pressure drop correlation was derived for finned metal foam heat sinks subject to uniform impinging air flow. The proposed correlations may be used in the design and optimization of finned metal foam heat sinks. By using the correlations, thermal performance of the finned metal foam heat sink was compared with the conventional plate-fin heat sink subject to uniform impinging air flow.

2 Modeling the Heat Transfer and Pressure Drop

With reference to Fig. 1(*a*), the problem under consideration was a finned metal foam heat sink subject to uniform impinging air jet. The jet nozzle was right on top of the foam tip, i.e., there was no flow bypass from the gap between the nozzle exit and the foam. The cooling air was uniformly discharged onto the heat sink with an approaching velocity V_0 and initial temperature T_0. Upon entering the heat sink, the flow area was reduced due to the blockage of the fins and hence the inlet velocity in the foam filled channel (V_{in}) was higher than the approaching velocity (V_0). The bottom substrate of the heat sink was heated at a constant temperature T_w. The two outside plate-fins (each having a thickness half that of the internal fins) were thermally insulated at the external surfaces. A unit cell of the heat sink may therefore be employed for analysis. The length, width, and height of the heat sink were L, W, and H, respectively, the width of the channel filled with aluminum foams was denoted by s, and the plate-fin thickness was represented by t, as shown schematically in Fig. 1(*b*). The plate-fins, the substrate, and the foam were all made of pure aluminum.

2.1 Mathematical Formulation.

In a finned metal foam heat sink, heat transfer in the plate-fins was coupled to that in the cellular foams. The standard heat conduction equation was used to describe the heat transfer in the plate-fins. Given the irregular structure of cellular foams, thermal fluid flow in metal foams was modeled using the porous medium approach.

In light of the symmetrical distribution of thermal-fluid flow in a fin–foam channel, only one quarter of the channel was considered in the computational domain, see Fig. 2. The computational domain included only the plate-fin and the porous foam region, as heat transfer in the substrate was not considered. This was considered reasonable because the thermal resistance across the substrate was negligible due to the high conductivity of aluminum.

In order to simplify the problem, several assumptions have been made in the numerical model. Contact resistance at the foam/fin interface may be ignored if the foam blocks are properly bonded to the fins through high conductivity thermal adhesive or brazing [30]. The cellular aluminum foam was assumed to be homogenous and isotropic. The flow was steady state, laminar, and incompressible. The thermophysical properties of both the fluid and the foam were independent of temperature. As air was used as the coolant, thermal dispersion in the foam can be ignored [16,31]. Contribution by thermal radiation was not considered. Based on these assumptions, the mathematical formulation may be written in tensor form as below.

Fluid flow in the porous foam was described using the Darcy's extended equation, as

$$\nabla \cdot \langle \mathbf{u} \rangle = 0 \tag{1}$$

$$\frac{\rho_f}{\varepsilon}\nabla(\langle \mathbf{u} \rangle \langle \mathbf{u} \rangle) = -\varepsilon \nabla \langle p \rangle^f + \mu_f \nabla^2 \langle \mathbf{u} \rangle - \frac{\varepsilon \mu_f}{K}\langle \mathbf{u} \rangle - \frac{\varepsilon \rho_f c_E}{\sqrt{K}}|\langle \mathbf{u} \rangle|\langle \mathbf{u} \rangle \tag{2}$$

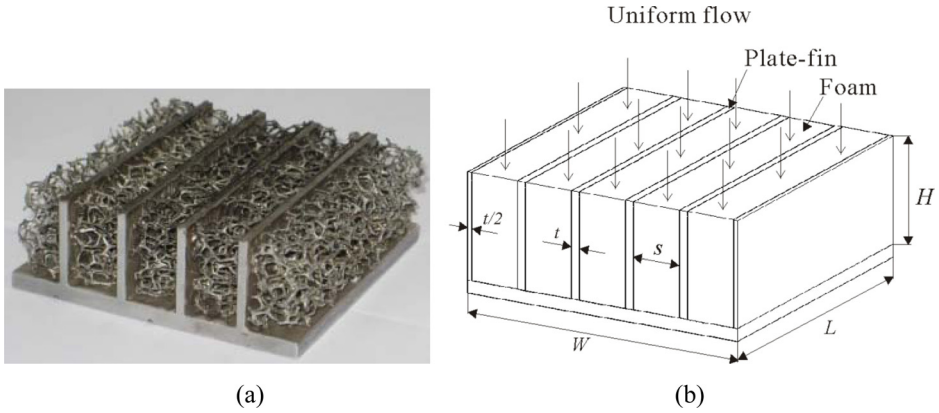

Fig. 1 Finned metal foam heat sink: (*a*) prototype and (*b*) schematic illustration

where the third term on the right-hand side (RHS) of Eq. (2) is the well known Darcy's term, the second and the last terms are the non-Darcy terms proposed by Vafai and Tien [32] to account for the boundary and inertial effects, K is the permeability, c_E is the form drag coefficient, and ε is the porosity.

Local thermal nonequilibrium between the two phases (i.e., solid and fluid phases) of the porous foam was assumed. Consequently, each phase may be described using a heat transfer equation as

$$k_{se}\nabla^2\langle T_s\rangle^s - h_{sf}A_{sf}(\langle T_s\rangle^s - \langle T_f\rangle^f) = 0 \tag{3}$$

$$\rho_f c_{p,f}\nabla\cdot\left(\langle\mathbf{u}\rangle\langle T_f\rangle^f\right) = k_{fe}\nabla^2\langle T_f\rangle^f + h_{sf}A_{sf}(\langle T_s\rangle^s - \langle T_f\rangle^f) \tag{4}$$

where ρ_f, $c_{p,f}$, and μ_f are separately the density, heat capacity, and viscosity of air; k_{fe} and k_{se} are the effective thermal conductivities of the fluid and solid phases, respectively; h_{sf} is the interstitial heat transfer coefficient between the two phases; and A_{sf} is the surface area density of the foam.

Coupled heat transfer in the plate-fin was governed by steady-state heat conduction equation, as

$$k_p\nabla^2 T_p = 0 \tag{5}$$

where k_p is the thermal conductivity of the plate-fin material.

It should be pointed out that, in Eqs. (1)–(5), $\langle\phi\rangle$denoted the extrinsic average of a quantity over a volume containing both the fluid and solid phases, and $\langle\phi\rangle^f$and $\langle\phi\rangle^s$ referred to the intrinsic averages over a volume containing only the fluid and solid phases, respectively. The extrinsic and intrinsic average of a generic transport variable was defined as

$$\langle\phi\rangle = \varepsilon\langle\phi\rangle^f, \langle\phi\rangle = (1-\varepsilon)\langle\phi\rangle^s \tag{6}$$

According to Feng et al. [30], convective heat dissipation at the inlet of the heat sink (including the fin tip and the foam region that was directly under jet impingement) should be considered. At heat sink inlet, i.e., $z = H$, for the foam region directly under jet impingement, the boundary condition applied was

$$\begin{aligned}&\langle u\rangle = \langle v\rangle = 0, \langle w\rangle = -V_{\text{in}},\\ &\langle T_f\rangle^f = T_0, -k_{se}\frac{\partial\langle T_s\rangle^s}{\partial z} = h_{\text{foam}}(\langle T_s\rangle^s - T_0)\end{aligned} \tag{7}$$

Again, at the heat sink inlet, for the fin tip directly under jet impingement

$$\langle u\rangle = \langle v\rangle = \langle w\rangle = 0, -k_p\frac{\partial T_p}{\partial z} = h_p(T_p - T_0) \tag{8}$$

At the exit of the heat sink, the local one-way behavior was assumed for u, v, w, and T_f [33]; the foam and the fin were considered to be thermally adiabatic as air was heated up upon penetrating the heat sink. These assumptions led to zero derivates specified for each quantities at the exit plane, i.e., $x = L/2$,

$$\frac{\partial\langle u\rangle}{\partial x} = \frac{\partial\langle v\rangle}{\partial x} = \frac{\partial\langle w\rangle}{\partial x} = 0, \quad \frac{\partial T_p}{\partial x} = \frac{\partial\langle T_s\rangle^s}{\partial x} = \frac{\partial\langle T_f\rangle^f}{\partial x} = 0 \tag{9}$$

At the symmetry plane of $x = 0$

$$\frac{\partial\langle v\rangle}{\partial x} = \frac{\partial\langle w\rangle}{\partial x} = 0, \quad \langle u\rangle = 0, \quad \frac{\partial T_p}{\partial x} = \frac{\partial\langle T_s\rangle^s}{\partial x} = \frac{\partial\langle T_f\rangle^f}{\partial x} = 0 \tag{10}$$

At the symmetry plane of $y = 0$

$$\frac{\partial\langle u\rangle}{\partial y} = \frac{\partial\langle w\rangle}{\partial y} = 0, \quad \langle v\rangle = 0, \quad \frac{\partial\langle T_s\rangle^s}{\partial y} = \frac{\partial\langle T_f\rangle^f}{\partial y} = 0 \tag{11}$$

At the symmetry plane of $y = s/2 + t/2$

$$\langle u\rangle = \langle v\rangle = \langle w\rangle = 0, \quad \frac{\partial T_p}{\partial y} = 0 \tag{12}$$

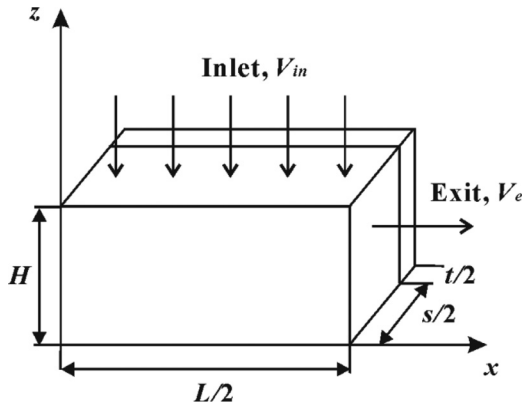

Fig. 2 Computational domain showing 1/4 of a fin–foam channel

At the bottom wall of $z = 0$

$$\langle u\rangle = \langle v\rangle = \langle w\rangle = 0, \quad T_p = \langle T_s\rangle^s = \langle T_f\rangle^f = T_w \tag{13}$$

At the interface between the solid plate-fin and the foam

$$\langle u\rangle = \langle v\rangle = \langle w\rangle = 0, \quad T_p = \langle T_s\rangle^s = \langle T_f\rangle^f, \quad -k_p\frac{\partial T_p}{\partial y} = -k_{se}\frac{\partial\langle T_s\rangle^s}{\partial y} - k_{fe}\frac{\partial\langle T_f\rangle^f}{\partial y} \tag{14}$$

As high porosity open-cell metal foams are composed of interconnected slender cylinders, the flow within the foam is similar to flow around staggered cylinders. The interstitial heat transfer coefficient was determined based on the correlation of staggered cylinders which had been validated for metal foams by Calmidi and Mahajan [31], as

$$Nu_{\text{foam}} = \frac{h_{\text{foam}}d_f}{k_f} = 0.52\text{Re}_d^{0.5}\text{Pr}^{0.37} \tag{15}$$

where Re_d is the Reynolds number based on foam ligament diameter and local velocity

$$\text{Re}_d = \frac{\rho_f|\langle\mathbf{u}\rangle|d_f}{\varepsilon\mu_f} \tag{16}$$

In Eq. (8), the convective heat transfer coefficient at the plate-fin tip was determined using the correlation of impinging flow on a flat plate [10,34], as

$$h_p = k_f/t\cdot 0.6\cdot\text{Re}_1^{0.5}, \quad \text{Re}_1 = \rho_f\cdot V_0\cdot t/\mu_f \tag{17}$$

2.2 Numerical Method and Model Parameters. The governing equations were solved using the finite-volume method. A staggered grid system was employed, where the velocities were stored at the control-volume faces; while, all other variables were calculated at the grid points. The numerical method used was based on the SIMPLE algorithm. The discretized equations for each variable were solved by the line-by-line procedure which is the combination of the Tri-Diagonal-Matrix Algorithm (TDMA) and the Gauss–Seidel iteration technique of Patankar [33]. The iteration was terminated when changes in target variables were less than 10^{-6} between successive iterations.

The present numerical model has been validated using the experimental data presented in Ref. [30], it was demonstrated that the model was adequate to simulate accurately both the pressure drop and heat transfer if the foam properties were exact. The validity of the present correlations is then determined mainly by the foam properties adopted. The foam properties adopted in the present numerical model were obtained through experimental measurements by Calmidi and Mahajan [31] (see Table 1), which were believed to be exact since the experimental measurements required no assumptions and approximations. The thermal conductivity of plate-fins used in the simulation was 218 W/m K. The density, viscosity, and thermal conductivity of air were 1.15463 kg/m^3, 1.824×10^{-5} kg/(m·s), and 0.02573 W/(m K), respectively. The Fortran code used for the computation has been tested and validated for several conjugated heat transfer problems [35,36].

2.3 Data Reduction. The Reynolds number may be defined based on the channel inlet velocity or channel exit velocity. For plate-fin heat sinks subject to impinging air cooling, Biber [6] and Duan and Muzychka [8] carried out analytical scaling analysis and found that the Nusselt number can be simply correlated as a function of the dimensionless developing flow length, with the Reynolds number defined based on the channel exit velocity. This suggested that the thermal-fluid flow behavior of a plate-fin heat sink subject to impinging jet cooling may be similar to that of a channel flow after impinging. Therefore, following Biber [6] and Duan and Muzychka [8], in the present study we used also the channel exit velocity to define the Reynolds number

$$\text{Re} = \frac{\rho_f V_e D_h}{\mu_f} \tag{18}$$

where D_h is the channel hydraulic diameter, $D_h = 2sH/(s+H)$, and, from mass conservation, $V_e = L/(2H)\times\cdot V_{\text{in}}$

The heat transfer coefficient and the Nusselt number were defined as

$$h = \frac{Q}{A_{\text{ch}}(T_w - T_0)} \quad \text{Nu} = \frac{hD_h}{k_f} \tag{19}$$

where A_{ch} is the fin surface area of a foam-filled channel, $A_{\text{ch}} = (s+2H)L$. Q is the total heat transfer rate from a foam-filled channel, which included both the heat transfer from the porous foam region and that from the plate-fins at the substrate.

$$Q = 4\cdot\left\{\iint_{A_{\text{foam}}}\left[-k_{se}\frac{\partial\langle T_s\rangle^s}{\partial z}\bigg|_{z=0} - k_{fe}\frac{\partial\langle T_f\rangle^f}{\partial z}\bigg|_{z=0}\right]dxdy + \iint_{A_{\text{fin}}}\left[-k_p\frac{\partial T_p}{\partial z}\bigg|_{z=0}\right]dxdy\right\} \tag{20}$$

Here, the multiplier "4" is attributed to the fact that the computational domain included only one-quarter of the unit cell; A_{foam} and A_{fin} are the base area of the foam and the plate-fin in the computational domain, respectively.

3 Results and Discussion

With the foam properties fixed, the main objective of the study was to quantify the effects of all relevant configurational parameters (channel length, channel width, fin thickness, and fin height) upon the thermal performance. Numerical simulations were carried out with different combinations of variables, the investigated range of each variable was listed in Table 2. Correlations were developed for the Nusselt number and pressure drop. By using the correlations, the thermal performance of the finned metal foam heat sink was compared with the conventional plate-fin heat sink.

3.1 Heat Transfer

3.1.1 Effect of L, s, t, and H. For heat transfer in plate-fin heat sinks subject to impinging jet cooling, Biber [6] and Duan and Muzychka [8] indicated that by proper use of the scaling, the data

Table 1 Thermal properties of open-cell aluminum foam [28]

Porosity	PPI	d_f (mm) fiber dia.	d_p (mm) pore dia.	c_E	K ($\times10^7$m^2)	k_{se} (W/m K)	k_{fe} (W/m K)	A_{sf} (m^2/m^3)
0.9118	5	0.55	3.8	0.085	1.8	6.46	0.0237	918

Table 2 Ranges of relevant heat sink variables considered

Variable	Low	High
L	40 mm	120 mm
H	10 mm	68 mm
S	3 mm	15 mm
T	1 mm	2 mm
V_0	0.5 m/s	3 m/s

points for varying geometrical parameters (e.g., channel length, channel width, and fin height) can be made to collapse onto one curve for the Nusselt number as a function of the developing flow length $(L/2)/(\mathrm{Re}D_h)$. Here, we selected also the $(L/2)/(\mathrm{Re}D_h)$ scaling as the independent parameter and plotted in Figs. 3–6 the Nusselt number as a function of $(L/2)/(\mathrm{Re}D_h)$ for varying L, s, t, and H, respectively. As shown in Fig. 3(*a*), when the fin height was relatively small, e.g., $H = 10$ mm, the Nusselt number corresponding to different channel lengths did collapse onto a single curve, consistent with the conventional plate-fin heat sink. However, as increasing the fin height, the curves for different channel lengths gradually deviated from each other, see Figs. 3(*b*)–3(*d*). This showed that for finned metal foam heat sink the Nusselt number did not obey a simple relationship with the developing flow length.

As shown in Fig. 4, the Nusselt number slightly increased as the channel width was increased at a given $(L/2)/(\mathrm{Re}D_h)$. As the channel width was increased, the hydraulic diameter increased accordingly to maintain $(L/2)/(\mathrm{Re}D_h)$ at a constant value, the Reynolds number (or impinging flow velocity) should be decreased, causing the Nusselt number to decrease. However, at the same time, the volume of the foam block in the channel increased with increasing the channel width, which increased the total heat transfer area. As a result, the Nusselt number slightly increased as the channel width increased due to the combined effects of the decreased Reynolds number and the increased heat transfer area.

With all the other parameters fixed, increasing the fin thickness led to higher fin efficiency and thereby higher heat transfer rate, see Fig. 5. Figure 5 further showed that the effect of fin thickness increased as the fin height was increased. This is because at low fin height the fin efficiency was already high with small fin thickness; therefore, the effect of increased fin efficiency by increasing the fin thickness was less important.

Figure 6 plotted the Nusselt number as a function of $(L/2)/(\mathrm{Re}D_h)$ with varying the fin height H. It was evident that at a given $(L/2)/(\mathrm{Re}D_h)$ value, the Nusselt number decreased as H was increased. The decrease in the Nusselt number may be caused partially by the decreased Reynolds number and partially by the decreased fin efficiency as H was increased.

3.1.2 Heat Transfer Correlation. Results in Figs. 3–6 demonstrated that the thermal characteristics of finned metal foam heat sink were more complex than the conventional plate-fin heat sink: the Nusselt number depended not only on the dimensionless developing flow length but also on the channel length, channel width, fin thickness, and fin height. This may be caused by the different heat dissipation mechanism in the finned metal foam heat sink, i.e., the heat was rejected from both the fin surface and the foam ligaments. Based on numerical data with many different combinations of variables, a correlation for Nusselt number of finned metal foam heat sinks as functions of configurational parameters may be proposed as

$$\mathrm{Nu} = a\left(\frac{t}{d_p}\right)^{n1}\left(\frac{L/2}{d_p}\right)^{n2}\left(\frac{s}{d_p}\right)^{n3}\left(\frac{L/2}{\mathrm{Re}D_h}\right)^{n4} \tag{21}$$

where the last term on the RHS is the dimensionless developing flow length which followed the definition in the correlation of

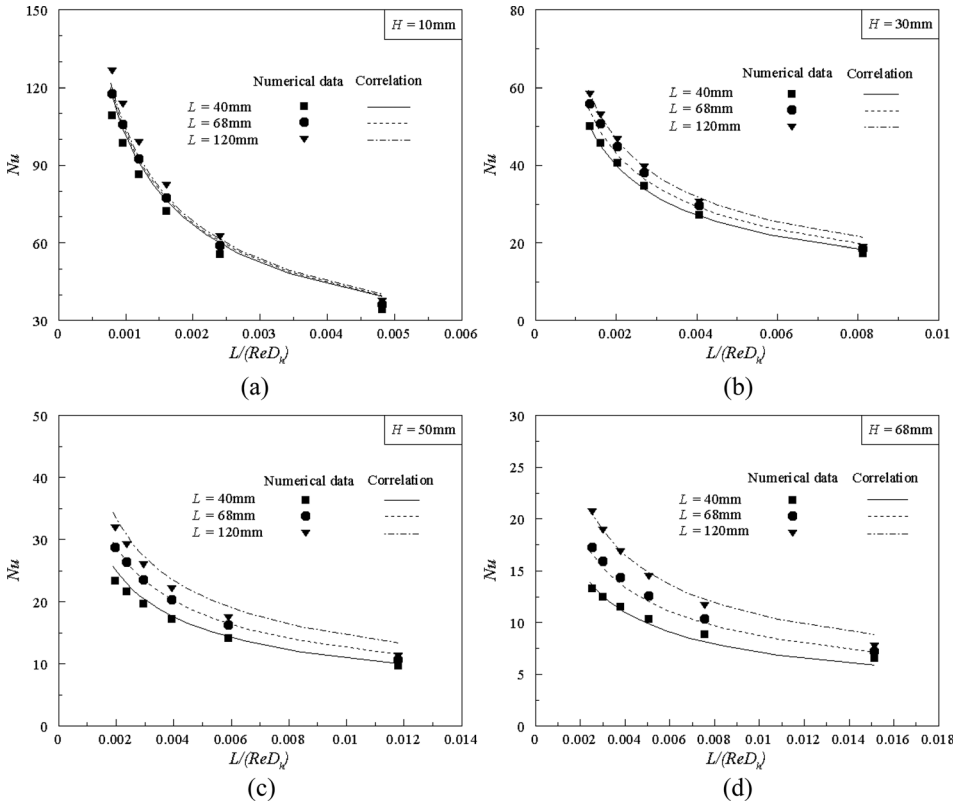

Fig. 3 Nusselt number plotted as a function of $(L/2)/(\mathrm{Re}D_h)$ for selected values of channel length L: (*a*) $H = 10$ mm; (*b*) $H = 30$ mm; (*c*) $H = 50$ mm; and (*d*) $H = 68$ mm, with $s = 6$ mm and $t = 1$ mm

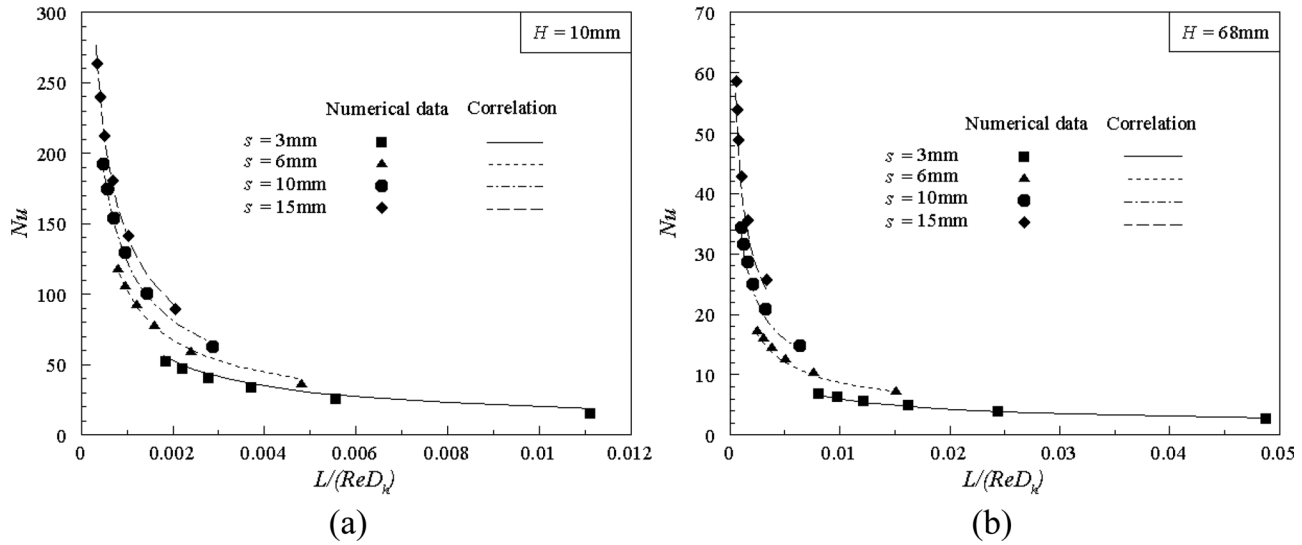

Fig. 4 Nusselt number plotted as a function of $(L/2)/(\mathrm{Re}D_h)$ for selected values of channel width s: (*a*) $H = 10$ mm and (*b*) $H = 68$ mm, with $L = 68$ mm and $t = 1$ mm

conventional plate-fin heat sink [6,8]. The first three terms were used to correct the influences of the fin thickness, channel length, and channel width, respectively. While the effect of fin height was combined into the coefficients of a, $n1$, $n2$, $n3$, and $n4$ in Eq. (21), these coefficients were correlated as a function of the fin height as

$$a = 1.5402 - 0.0539\left(\frac{H}{d_p}\right) \tag{22}$$

$$n1 = 0.1671 \ln\left(\frac{H}{d_p}\right) - 0.0858 \tag{23}$$

$$n2 = 0.0229\left(\frac{H}{d_p}\right) - 0.0376 \tag{24}$$

$$n3 = 0.2811\left(\frac{H}{d_p}\right)^{0.2229} \tag{25}$$

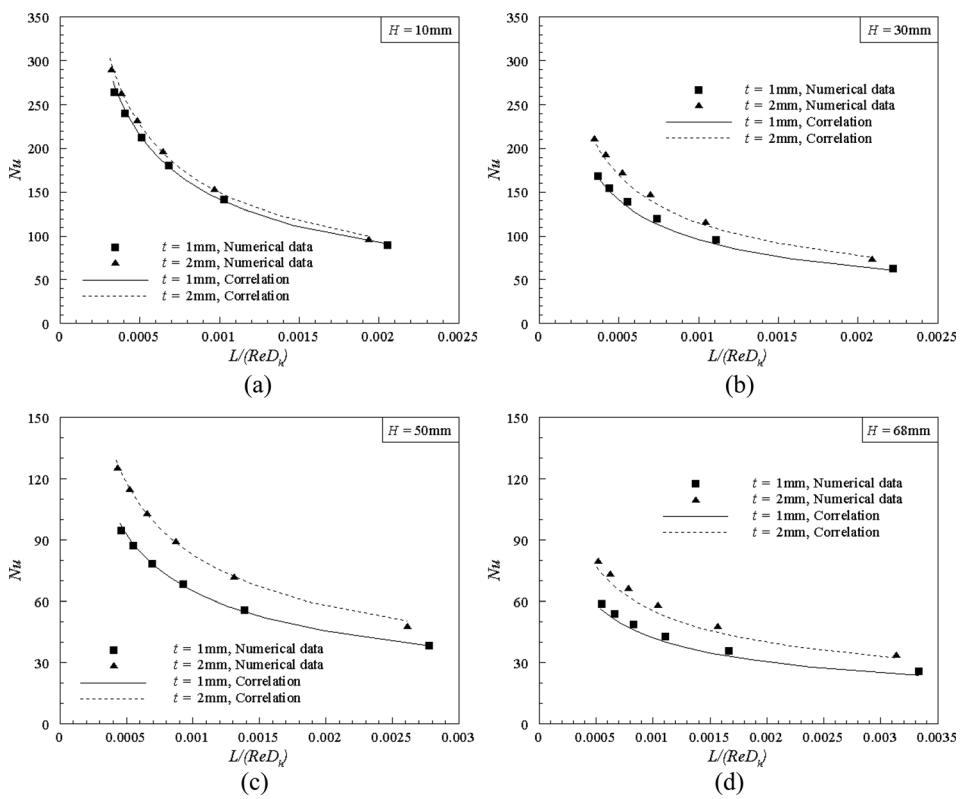

Fig. 5 Nusselt number plotted as a function of $(L/2)/(\mathrm{Re}D_h)$ for selected values of fin thickness t: (*a*) $H = 10$ mm; (*b*) $H = 30$ mm; (*c*) $H = 50$ mm; and (*d*) $H = 68$ mm, with $s = 15$ mm and $L = 68$ mm

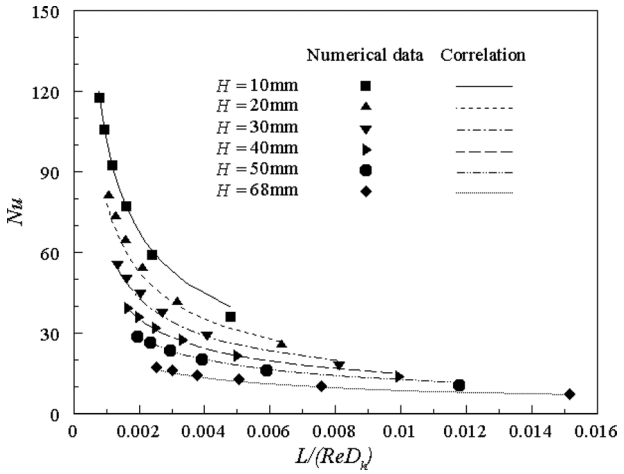

Fig. 6 Nusselt number plotted as a function of (L/2)/(ReD_h) for selected values of heat sink height H, with $s = 6$ mm, $L = 68$ mm, and $t = 1$ mm

$$n4 = 0.0087\left(\frac{H}{d_p}\right) - 0.6296 \tag{26}$$

In the investigated range of fin height $n1$, $n2$, and $n3$ were all positive, indicating that the Nusselt number increased as increasing the fin thickness, channel length, and channel width when plotted as a function of the dimensionless developing flow length (see Figs. 3–5). While $n4$ was always negative, it was consistent with the decreasing trends of the curves in Figs. 3–6.

The Nusselt number correlation of Eq. (21) was valid within the following range of parameters: $1\,\text{mm} \le t \le 2\,\text{mm}$, $40\,\text{mm} \le L \le 120\,\text{mm}$, $10\,\text{mm} \le H \le 68\,\text{mm}$, $3\,\text{mm} \le s \le 15\,\text{mm}$, and $0 \le V_{\text{in}} \le 5$ m/s. The correlation fitted the numerical results within ± 14%, see the comparisons between the numerical data and the correlation in Figs. 3–6.

3.2 Pressure Drop. The pressure drop of a finned metal foam heat sink was consisted of three terms: pressure drop in the foam-filled channel (Δp_{ch}), pressure drop at the heat sink inlet (Δp_i), and pressure drop at the exit (Δp_e), namely,

$$\Delta p = \Delta p_{\text{ch}} + \Delta p_i - \Delta p_e \tag{27}$$

The last two terms were caused by the contraction and expansion of the flow associated with entering and exiting the heat sink and will be determined based on correlations. At this stage, let us simply forget about them. Consider then the first term, i.e., pressure drop in the foam-filled channel, which can be obtained directly from the numerical solution of the governing equations (1) and (2), as

$$\Delta p_{\text{ch}} = \frac{1}{A_i}\iint_{A_i} p(x,y,H)dxdy - \frac{1}{A_e}\iint_{A_e} p(L/2,y,z)dydz \tag{28}$$

where A_i denotes the inflow surface area and A_e is the outflow surface area.

Next, we will mathematically develop a correlation for Δp_{ch} and compare it with the numerical simulation data of Eq. (28). The pressure drop in the foam-filled channel was induced by two different mechanisms: channel wall friction and bulk resistance of the porous foam. Amongst the two mechanisms, the channel wall friction may be negligible compared to the bulk resistance of the porous foam. The supporting evidence was presented in Fig. 7, which plotted the pressure drop in the foam-filled channel (Δp_{ch}) as a function of channel inlet velocity for selected channel widths. The channel width was larger, contribution of the wall friction to Δp_{ch} became less. As shown in Fig. 7, Δp_{ch} was almost not affected by the channel width, although it decreased slightly with increasing the channel width, indicating that the channel wall friction was negligible.

Given that the channel wall friction was negligible, we can consider the limiting case with infinitely large channel width, i.e., a metal foam block without fins subject to uniform impinging jet as shown in Fig. 8 to derive a correlation for Δp_{ch}. In this case, the problem was simplified to be two dimensional. In order to derive a correlation for Δp_{ch} mathematically, the stream function of an impinging flow in cellular foam was assumed to be that of an inviscid flow near the stagnation point over a flat plate [12]

$$\langle u \rangle = \frac{V_{\text{in}}}{H}x \quad \langle w \rangle = -\frac{V_{\text{in}}}{H}z \tag{29}$$

The justification for using the inviscid flow distribution will be discussed later.

Substituting Eq. (29) into the momentum equation for porous foam, i.e., Eq. (2), and further assuming that $|\langle \mathbf{u} \rangle| = \sqrt{\langle u \rangle^2 + \langle w \rangle^2} \approx |\langle u \rangle|$ for the x momentum equation and $|\langle \mathbf{u} \rangle| \approx |\langle w \rangle|$ for the z momentum equation, one gets

$$\frac{\varepsilon^2}{\rho}\frac{\partial p}{\partial x} = c_1 x - c_2 x^2 \tag{30}$$

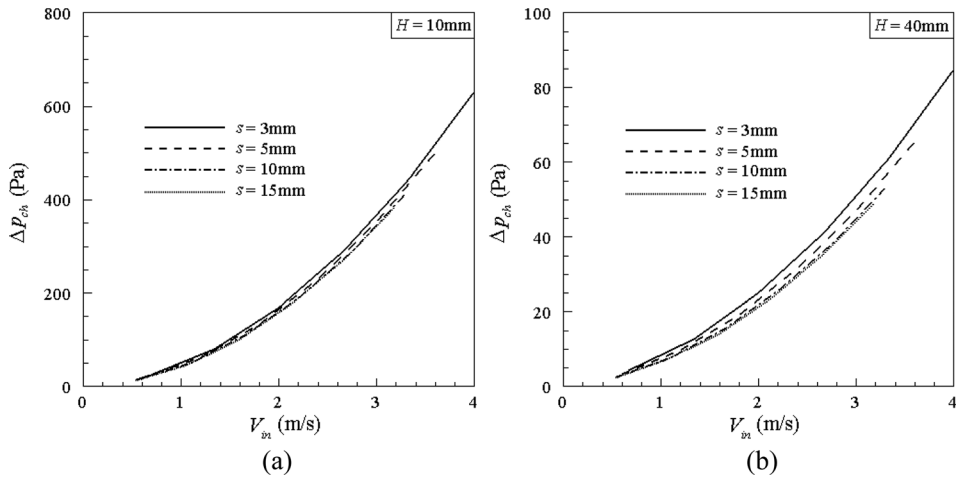

Fig. 7 Effect of channel width on pressure drop in foam-filled channel: (*a*) $H = 10$ mm and (*b*) $H = 40$ mm

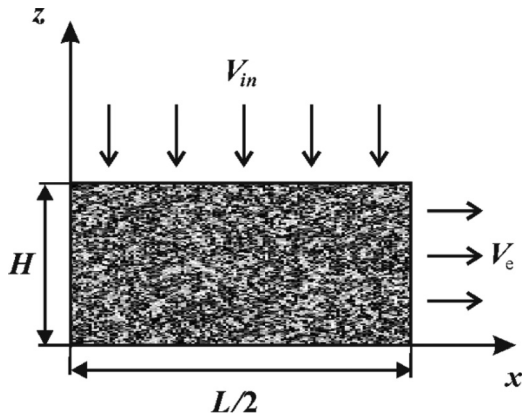

Fig. 8 Metal foam subjected to uniform impinging flow

$$\frac{\varepsilon^2}{\rho}\frac{\partial p}{\partial z} = c_3 z + c_2 z^2 \tag{31}$$

where

$$c_1 = -\frac{V_{\text{in}}^2}{H^2} - \frac{\varepsilon^2 \upsilon_f}{K}\frac{V_{\text{in}}}{H}, \quad c_2 = \frac{\varepsilon^2 c_E}{\sqrt{K}}\frac{V_{\text{in}}^2}{H^2}, \quad c_3 = -\frac{V_{\text{in}}^2}{H^2} + \frac{\varepsilon^2 \upsilon_f}{K}\frac{V_{\text{in}}}{H} \tag{32}$$

Integrating both sides of Eq. (30) with respect to x yielded

$$\frac{\varepsilon^2}{\rho}p(x,z) = \frac{c_1}{2}x^2 - \frac{c_2}{3}x^3 + g(z) \tag{33}$$

Differentiating Eq. (33) with respect to z led to

$$\frac{\varepsilon^2}{\rho}\frac{\partial p}{\partial z} = g'(z) \tag{34}$$

Substitution of Eq. (34) into Eq. (31) resulted in

$$g'(z) = c_3 z + c_2 z^2 \tag{35}$$

Integrating both sides of Eq. (35) with respect to z, one obtained

$$g(z) = \frac{c_3}{2}z^2 + \frac{c_2}{3}z^3 \tag{36}$$

By combining Eq. (36) with Eq. (33), the pressure distribution was obtained as

$$\frac{\varepsilon^2}{\rho}p(x,z) = \frac{c_1}{2}x^2 - \frac{c_2}{3}x^3 + \frac{c_3}{2}z^2 + \frac{c_2}{3}z^3 \tag{37}$$

Finally, the pressure drop in the foam-filled channel became

$$\begin{aligned}\Delta p_{\text{ch}} &= \frac{1}{L/2}\int_0^{L/2} p(x,H)dx - \frac{1}{H}\int_0^{H} p(L/2,z)dz \\ &= \frac{\rho}{\varepsilon^2}\left\{\left[\frac{1}{4}\frac{\varepsilon^2 c_E}{\sqrt{K}}\left(H + \frac{(L/2)^3}{H^2}\right) + \frac{1}{3}\left(\frac{L/2}{H}\right)^2 - \frac{1}{3}\right]V_{\text{in}}^2 \right. \\ &\quad \left. + \frac{1}{3}\frac{\varepsilon^2 \upsilon_f}{K}\left(\frac{(L/2)^2}{H} + H\right)V_{\text{in}}\right\}\end{aligned} \tag{38}$$

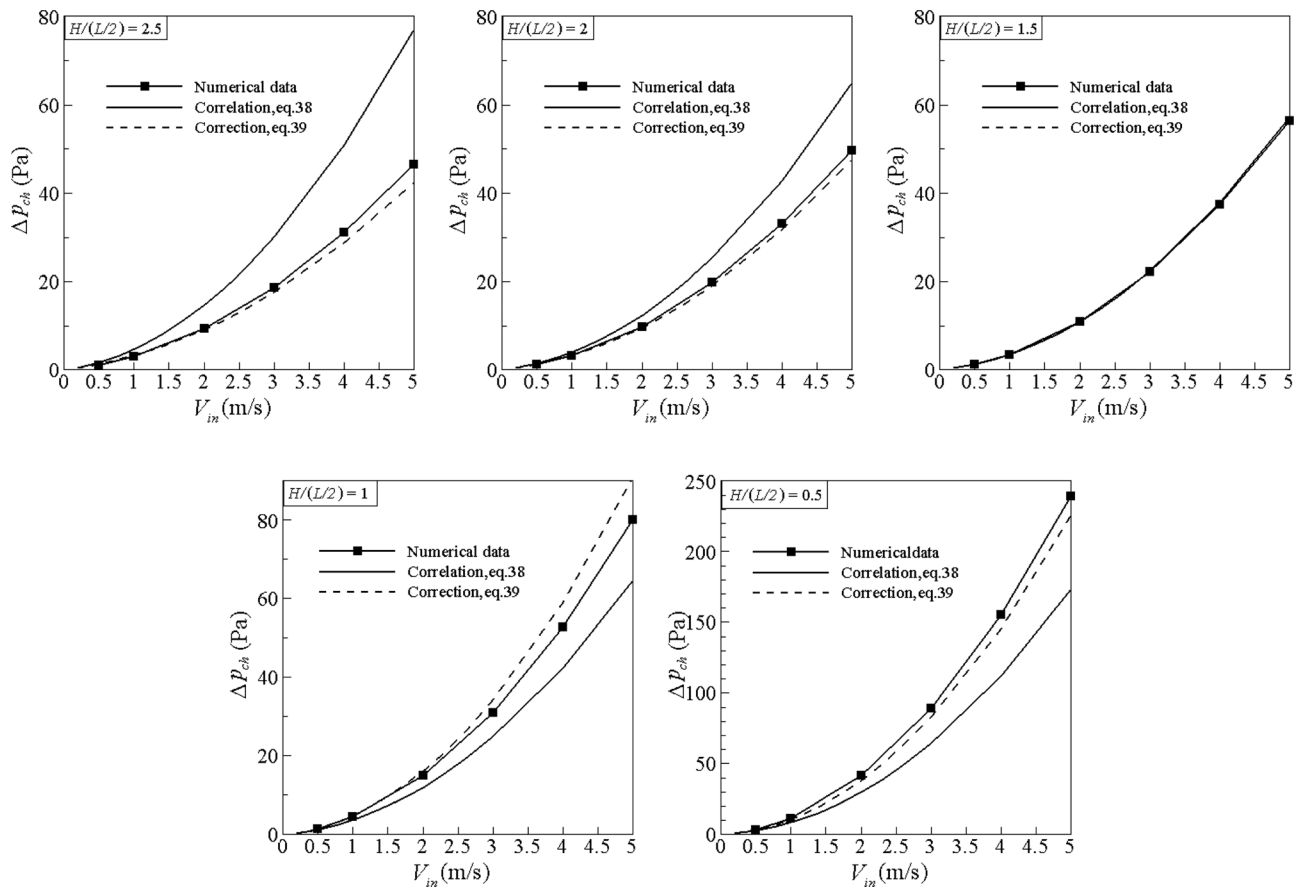

Fig. 9 Comparison of pressure drop between full numerical simulation and correlations for $L = 40$ mm

The correlation given in Eq. (38) was compared with full numerical simulation for verification, comparison results were shown in Figs. 9–11 for $L = 40$ mm, 68 mm, and 120 mm, respectively. It was found that the correlation overpredicted the pressure drop when $H/(L/2) > 1.5$ and underpredicted the pressure drop when $H/(L/2) < 1.5$. A correction of Eq. (38) may be made as

$$\Delta p_{\text{ch}} = \frac{\rho}{\varepsilon^2}\left\{\left[\frac{1}{4}\frac{\varepsilon^2 c_E}{\sqrt{K}}\left(H + \frac{(L/2)^3}{H^2}\right) + \frac{1}{3}\left(\frac{L/2}{H}\right)^2 - \frac{1}{3} + C\left(1.5 - \frac{H}{L/2}\right)\right]V_{\text{in}}^2 + \frac{1}{3}\frac{\varepsilon^2 \upsilon_f}{K}\left(\frac{(L/2)^2}{H} + H\right)V_{\text{in}}\right\} \tag{39}$$

$$(C = 1 \text{ when } H/L > 0.75)$$

$$(C = 1.5 \text{ when } H/L < 0.75)$$

Equation (39) predicted the pressure drop within ± 15% of the numerical results for $0 < H/L \le 1$, $40\,\text{mm} \le L \le 120\,\text{mm}$, and $0 < V_{\text{in}} < 5$ m/s.

Figures 12(*a*) and 12(*b*) presented typical streamlines distribution for inviscid flow and actual flow in cellular foam, respectively. The inviscid flow did not include the boundary viscous effect of the impinging plate as well as the influence of cellular foam on the velocity distribution. The deviation of Eq. (38) from numerical simulations may be affected by the difference between the inviscid flow and the actual flow in cellular foam. For example, more air will escape from the side (*x*-direction in Fig. 8) in the top half of the foam due to the flow resistance caused by the foam; while for the inviscid impinging flow, the air will uniformly escape from the side along the height direction. However, the present exercise proved that using the inviscid impinging flow for approximation is acceptable for the investigated high porosity foam. The same approximation was also proved for plate-fin heat sinks subjected to uniform impinging air jet in Ref. [12]. For air flow passing through a straight pipe filled with porous foam, the pressure drop was dependent mainly upon the mean flow velocity, the flow length, and the foam properties, but less upon the velocity profile inside the pipe since wall friction was negligible compared to bulk foam resistance. Similar behavior was expected for impinging flow in metal foam. One can assume that each streamline in Fig. 12 was the flow inside a bended tube, the overall pressure drop was then determined by the length of each bended tube, the mean flow velocity inside the tube, and the foam properties. As shown in Fig. 12(*a*), the shape and distribution of the "bended tubes" (i.e., streamlines) for the inviscid impinging flow did capture the essential features of the flow in metal foam shown in Fig. 12(*b*). Therefore, using the inviscid flow distribution for the flow in metal foam led to acceptable predictions of pressure drop.

Now that the pressure drop in the foam-filled channel was determined, consider next the pressure drop at the heat sink inlet and exit, see Eq. (27). Although the two terms contributed less than 5% to the total pressure drop, their correlations were presented here for completeness. The pressure drop at the inlet had two terms, namely, flow acceleration and an irreversible loss term associated with free expansion [7]

$$\Delta p_i = \left[\left(1 - \sigma^2\right) + K_C\right] \times \frac{1}{2}\rho_f V_{\text{in}}^2 \tag{40}$$

Similarly, the pressure rise at the exit consisted of a flow deceleration term and a loss coefficient, given by

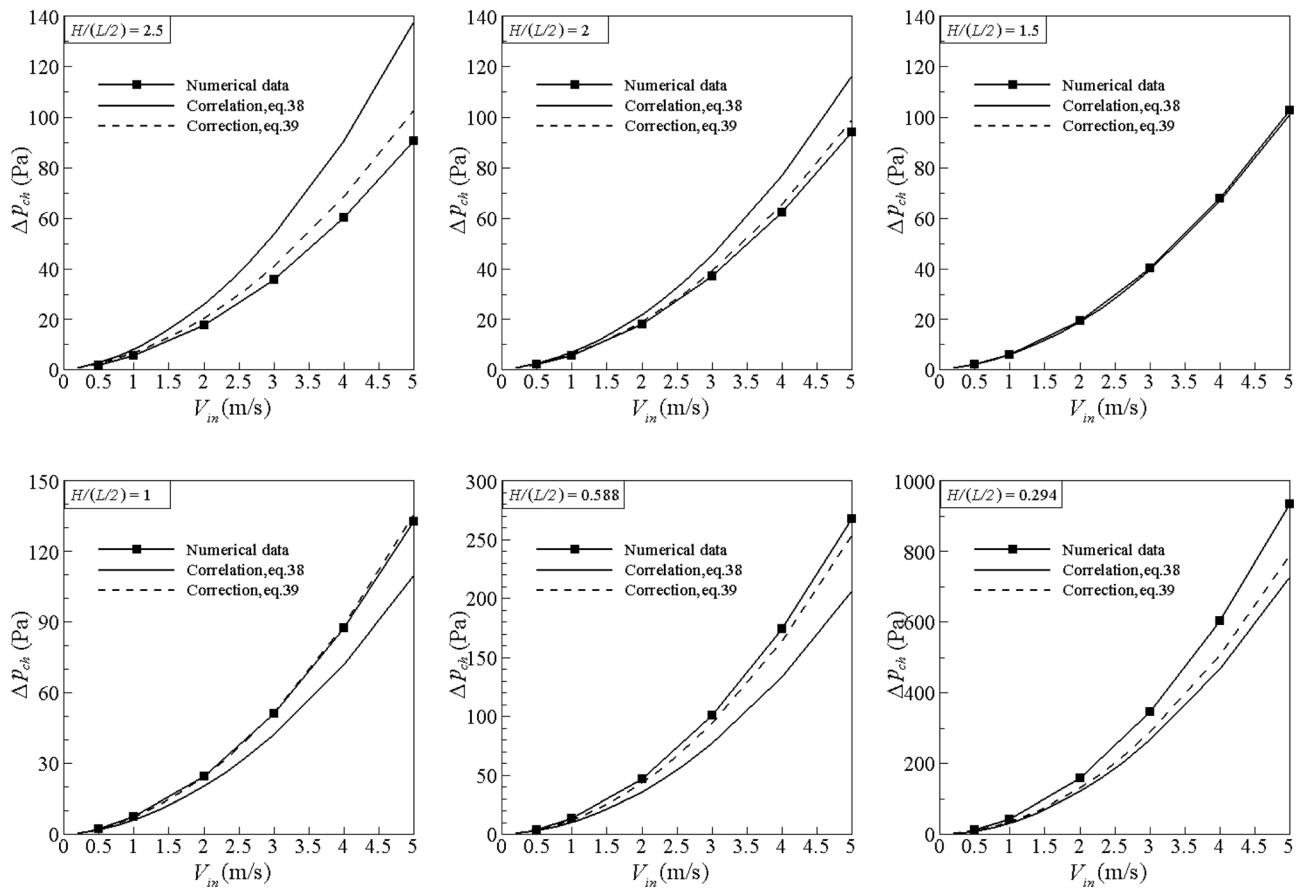

Fig. 10 Comparison of pressure drop between numerical simulation and correlations for $L = 68$ mm

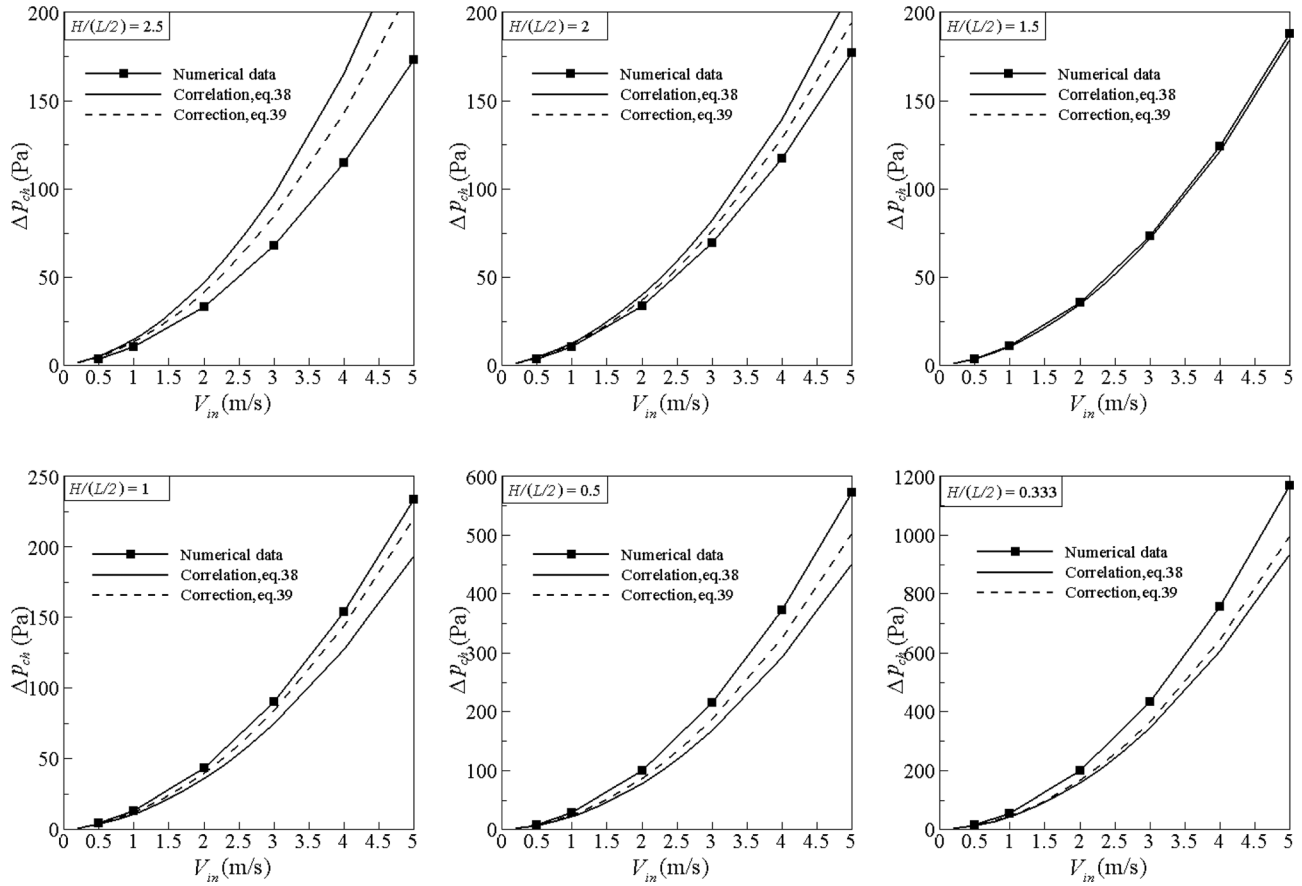

Fig. 11 Comparison of pressure drop between full numerical simulation and correlations for $L = 120$ mm

$$\Delta p_e = \left[\left(1-\sigma^2\right) - K_e\right] \times \frac{1}{2}\rho_f V_e^2 \tag{41}$$

where $\sigma = s/(s+t)$ is the area contraction ratio; K_c and K_e are separately the inlet and exit loss coefficients, which were estimated using an equation experimentally derived by Jeng and Tzeng [37] and Mills [38], as

$$K_C = 0.4 \times (1-\sigma^2) + \beta \tag{42}$$

$$K_e = (1-\sigma)^2 - \beta \times \sigma \tag{43}$$

$$\beta = \begin{array}{l} -0.01 \cdot (C-57) + 0.79, (\mathrm{Re}_{Dh} < 2\times 10^3) \\ -0.002 \cdot (C-57) + 0.18, (2\times 10^3 \le \mathrm{Re}_{Dh} < 6\times 10^3) \\ 0.0015 \cdot (C-57) + 0.12, (6\times 10^3 \le \mathrm{Re}_{Dh} < 6\times 10^4) \\ 0, (\mathrm{Re}_{Dh} \ge 6\times 10^4) \end{array} \tag{44}$$

$$C = 31.72 \cdot \left(\frac{D_h}{s}\right)^2 - 55.85 \cdot \left(\frac{D_h}{s}\right) + 80.94 \tag{45}$$

The hydraulic diameter D_h in Eq. (45) was different for the inlet ($=2 \cdot Ls/(L+s)$) and the exit channel ($=2 \cdot Hs/(H+s)$). Accordingly, the Reynolds number (Re_{Dh}) was different for the inlet ($= \rho_f V_{in} D_h/\mu_f$) and the exit channel ($= \rho_f V_e D_h/\mu_f$).

3.3 Comparison With Plate-Fin Heat Sinks. Kim et al. [11] developed analytical models to predict the thermal resistance and pressure drop of conventional plate-fin heat sinks subject to uniform impinging flow. Their models were applicable in the laminar flow range and experimentally validated for approaching velocity ranging from 0 to 2 m/s. The study also tabulated the optimum combination of fin thickness and channel width to minimize the thermal resistance under given pumping powers. The analytical models in Kim et al. [11] were used for plate-fin heat sinks in the comparison, while the proposed correlations in Eqs. (21) and (39) were used for finned metal foam heat sinks. Since the thermal performance of plate-fin heat sink was measured in thermal resistance, the heat transfer coefficient defined in Eq. (19) was converted to the thermal resistance accordingly.

$$R = \frac{\Delta T}{Q_t} = \frac{T_w - T_0}{N_f h A_{\mathrm{ch}} (T_w - T_0)} = \frac{1}{N_f h A_{\mathrm{ch}}} \tag{46}$$

where Q_t ($=N_f.Q$) is the total heat dissipation rate from a finned metal foam heat sink, and N_f is the number of fins or unit cells, $N_f = W/(s+t)$.

Figure 13 presented the thermal resistance of plate-fin heat sinks varying with fin numbers with the fin thickness fixed at 1 mm. The thermal resistances of finned metal foam heat sinks with 4, 6, 8, and 10 fins were also included in the figure for

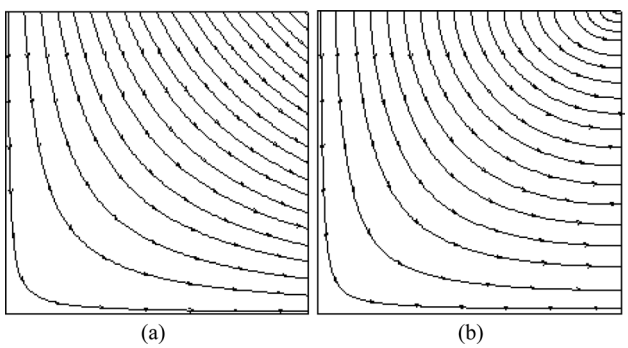

Fig. 12 Streamlines distribution for (*a*) inviscid impinging flow and (*b*) impinging flow in metal foam ($H/L = 0.5$ and $V_{\mathrm{in}} = 3$ m/s)

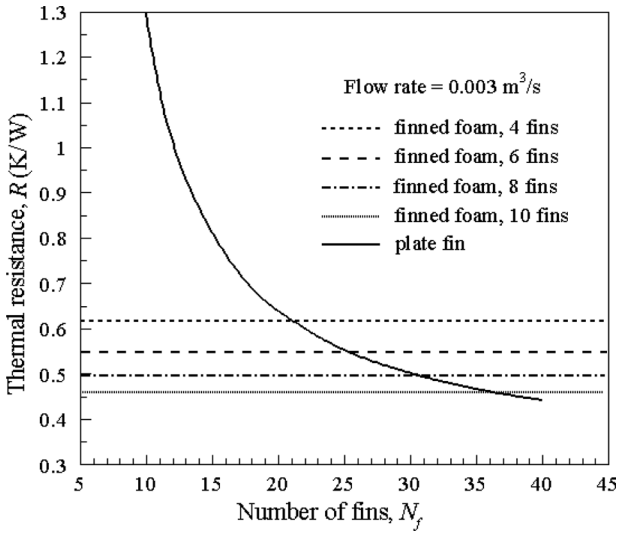

Fig. 13 Thermal resistance of plate-fin heat sinks plotted as a function of fin number in comparison with that of fined metal foam heat sinks having 4, 6, 8, and 10 fins ($t = 1$ mm, $L = W = 50$ mm, and $H = 25$ mm)

comparison. The overall dimensions of both heat sink types were fixed at 50 mm (length) × 50 mm (width) × 25 mm (fin height). As shown in Fig. 13, the thermal resistance of both heat sink types decreased as the number of fins was increased. The thermal resistance of finned metal foam heat sinks with 4, 6, 8, and 10 fins (or, equivalently, $s = 11.5$, 7.33, 5.25, and 4 mm) was comparable to that of plate-fin heat sinks with 21, 25, 30, and 36 fins ($s = 1.38$, 1, 0.67, and 0.39 mm), respectively. In other words, the finned metal foam heat sink can attain similar heat transfer with less fins, thereby saving the material consumption and reducing the weight of heat sink. For example, with the same heat dissipation rate, the weight of the finned metal foam heat sink was only ~1/3 of the plate-fin heat sink.

Figure 14 compared the pressure drop of the two heat sink types at selected fin numbers with the flow rate varied from 0 to 0.005 m^3/s (or approaching velocity 0–2 m/s). It was found that the pressure drop of both heat sink types increased with increasing fin number. The pressure drop of the plate-fin heat sink with 21 fins was comparable to that of the finned metal foam heat sink with 10 fins, whereas the finned metal foam heat sink with 10 fins

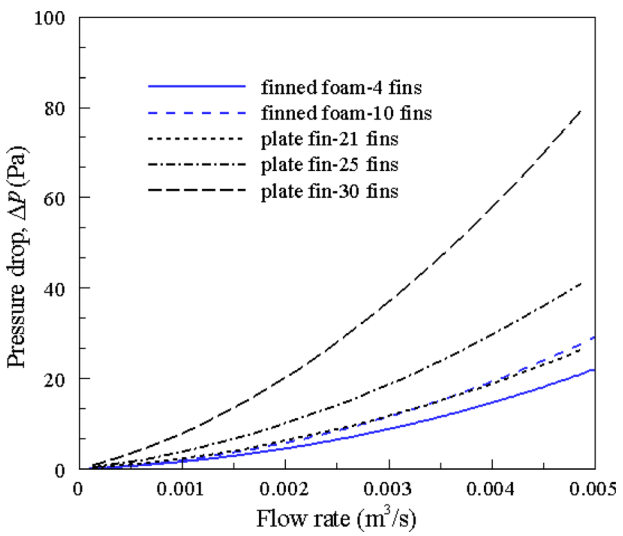

Fig. 14 Comparison of pressure drop between plate-fin heat sinks and fined metal foam heat sinks ($t = 1$ mm, $L = W = 50$ mm, and $H = 25$ mm)

Table 3 Thermal resistance comparison between plate-fin heat sinks and finned metal foam heat sinks at a given pumping power of 0.0164 W ($L = W = 50$ mm, $H = 25$ mm)

Type of heat sink	Fin thickness, t (mm)	Fin gap, s mm)	Number of fins, N_f	Thermal resistance, R(K/W)
Finned foam	1	11.5	4	0.685
Finned foam	1	7.33	6	0.617
Finned foam	1	5.25	8	0.571
Finned foam	1	4	10	0.539
Plate-fin	1	4	10	1.234
Plate-fin	1	1.94	17	0.769
Plate-fin	1	1.5	20	0.729
Plate-fin	1	1.08	24	0.734
Plate-fin	1	0.56	32	0.940
Plate-fin[a]	0.207	0.884	46	0.553

[a]Plate-fin heat sink with fully optimized fin thickness and channel width [8].

had much smaller thermal resistance than the plate-fin heat sink with 21 fins (see Fig. 13).

The thermal performance of finned metal foam heat sinks was further compared with that of plate-fin heat sinks on a given pumping power basis. With the fin thickness set to be 1 mm (which is common for commercially available plate-fin heat sinks), Table 3 showed that there existed an optimal channel width (or optimal fin number) ~ 1.5 mm for plate-fin heat sinks. When the fin thickness and channel width were both optimized for plate-fin heat sinks, Kim et al. [11] found that $t = 0.207$ mm and $s = 0.884$ mm were ideal, which may be regarded as a microchannel heat sink [12,39]. Under a given pumping power, the thermal resistance of the finned metal foam heat sink with 10 fins was 26% lower than the optimal plate-fin heat sink of conventional size ($t = 1$ mm and $s = 1.5$ mm), and 2.5% lower than the fully optimized plate-fin heat sink ($t = 0.207$ mm and $s = 0.884$ mm). If the fin thickness was simultaneously optimized for finned metal foam heat sinks, the thermal performance could be further enhanced. Furthermore, the fully optimized microchannel plate-fin heat sink was mechanically weaker due to the very thin plate-fins compared to the investigated finned metal foam heat sinks. In practical applications, the selection of a heat sink type should comprehensively consider the thermal performance, manufacturing cost, weight and volume, and sometimes the mechanical properties as well.

4 Conclusions

Heat transfer and pressure drop characteristics of finned metal foam heat sinks subject to uniform impinging air flow were numerically investigated. Effects of the channel length, channel width, fin thickness, and fin height were examined upon the thermal performance. It was found that the Nusselt number increased as increasing the fin thickness, channel width, and channel length, whereas declined as increasing the fin height at a given dimensionless developing flow length. Correlations were developed for the Nusselt number and pressure drop, which may be used in the design and optimization of finned metal foam heat sinks under impinging flow.

The thermal performance of the fined metal foam heat sinks was compared to the conventional plate-fin heat sinks having the same volume. With the flow rate fixed, to attain the same heat transfer rate the weight of the finned metal foam heat sink was only ~1/3 of the plate-fin heat sink. On a given pumping power basis, the thermal resistance of the finned metal foam heat sink with 10 fins was 26% lower than the optimal plate-fin heat sink of conventional size (fin thickness $t = 1$ mm and channel width $s = 1.5$ mm), and 2.5% lower than the fully optimized microchannel plate-fin heat sink ($t = 0.207$ mm and $s = 0.884$ mm).

Acknowledgment

This work was supported by the National Natural Science Foundation of China (51206128), the National Basic Research

Program of China (2011CB610305), the National "111" Project of China (B06024), China Postdoctoral Science Foundation funded project (2012M521766), Shaanxi Province Science Foundation funded project, and the Fundamental Research Funds for the Central Universities of China.

Nomenclature

A_{ch} = surface area of a fin–foam channel (m^2)
A_{sf} = wetted surface area per volume (m^2/m^3)
c_E = form drag coefficient
c_p = heat capacity (J/kg K)
d_f = fiber diameter of metal foam (mm)
D_h = hydraulic diameter (mm)
d_p = pore diameter of metal foam (mm)
h = heat transfer coefficient (W/m^2 K)
H = height of heat sink (mm)
h_{sf} = interstitial heat transfer coefficient (W/m^2 K)
k = thermal conductivity (W/m K)
K = permeability (m^2)
L = length of heat sink (mm)
Pr = Prandtl number
Q = heat transfer rate (W)
R = thermal resistance (K/W)
Re = Reynolds number
s = channel width (mm)
t = fin thickness (mm)
T_w = substrate temperature (K)
T_0 = inlet temperature of air (K)
V_e = exit channel velocity (m/s)
V_{in} = inlet channel velocity ($= V_0/\sigma$) (m/s)
V_0 = approaching velocity of air (m/s)
W = width of heat sink (mm)
Δp = pressure drop (Pa)

Greek Symbols

ε = porosity
μ = viscosity (kg/ms)
ρ = density (kg/m^3)
σ = area contraction ratio ($=s/(s+t)$)

Subscripts

f = fluid-phase
p = plate-fins
s = solid-phase

References

[1] Nakayama, W., 2013, "Heat in Computers: Applied Heat Transfer in Information Technology," ASME J. Heat Transfer, **136**(1), p. 013001.
[2] Ranjan, R., Turney, J. E., Lents, C. E., and Faustino, V. H., 2014, "Design of Thermoelectric Modules for High Heat Flux Cooling," ASME J. Electron. Packag., **136**(4), p. 041001.
[3] Ellsworth, J. M. J., Zoodsma, R. J., Cascio, F., and Behrendt, E., 2014, "Design and Control of the IBM Power 775 Supercomputer Water Conditioning Unit," ASME J. Electron. Packag., **136**(4), p. 041009.
[4] Bar-Cohen, A., Matin, K., Jankowski, N., and Sharar, D., 2014, "Two-Phase Thermal Ground Planes: Technology Development and Parametric Results," ASME J. Electron. Packag., **137**(1), p. 010801.
[5] Geb, D., and Catton, I., 2013, "Nonlocal Modeling and Swarm-Based Design of Heat Sinks," ASME J. Heat Transfer, **136**(1), p. 011401.
[6] Biber, C. R., 1997, "Pressure Drop and Heat Transfer in an Isothermal Channel With Impinging Flow," IEEE Trans. Compon. Packag. Manuf. Technol. Part A, **20**(4), pp. 458–462.
[7] Saini, M., and Webb, R. L., 2002, "Validation of Models for Air Cooled Plane Fin Heat Sinks Used in Computer Cooling," Eighth Intersociety Conference on Thermal and Thermomechanical Phenomena in Electronic Systems, (ITHERM 2002), San Diego, CA, June 1, pp. 243–250.
[8] Duan, Z., and Muzychka, Y. S., 2005, "Experimental Investigation of Heat Transfer in Impingement Air Cooled Plate Fin Heat Sinks," ASME J. Electron. Packag., **128**(4), pp. 412–418.
[9] Duan, Z., and Muzychka, Y. S., 2006, "Pressure Drop of Impingement Air Cooled Plate Fin Heat Sinks," ASME J. Electron. Packag., **129**(2), pp. 190–194.
[10] Kondo, Y., Behnia, M., Nakayama, W., and Matsushima, H., 1998, "Optimization of Finned Heat Sinks for Impingement Cooling of Electronic Packages," ASME J. Electron. Packag., **120**(3), pp. 259–266.
[11] Kim, D. K., Kim, S. J., and Bae, J. K., 2009, "Comparison of Thermal Performances of Plate-Fin and Pin-Fin Heat Sinks Subject to an Impinging Flow," Int. J. Heat Mass Transfer, **52**(15–16), pp. 3510–3517.
[12] Jang, S. P., and Kim, S. J., 2005, "Fluid Flow and Thermal Characteristics of a Microchannel Heat Sink Subject to an Impinging Air Jet," ASME J. Heat Transfer, **127**(7), pp. 770–779.
[13] Do, K. H., Kim, T. H., and Kim, S. J., 2010, "Analytical and Experimental Investigations on Fluid Flow and Thermal Characteristics of a Plate-Fin Heat Sink Subject to a Uniformly Impinging Jet," Int. J. Heat Mass Transfer, **53**(9–10), pp. 2318–2323.
[14] Hwang, G. J., Wu, C. C., and Chao, C. H., 1995, "Investigation of Non-Darcian Forced-Convection in An Asymmetrically Heated Sintered Porous Channel," ASME J. Heat Transfer, **117**(3), pp. 725–732.
[15] Kuo, S. M., and Tien, C. L., 1988, "Heat Transfer Augmentation in a Foam-Material Filled Duct With Discrete Heat Sources," Intersociety Conference on IEEE Thermal Phenomena in the Fabrication and Operation of Electronic Components (I-THERM '88), Los Angeles, CA, May 11–13, pp. 87–91.
[16] Hunt, M. L., and Tien, C. L., 1988, "Effects of Thermal Dispersion on Forced-Convection in Fibrous Media", Int. J. Heat Mass Transfer, **31**(2), pp. 301–309.
[17] Lu, T. J., 2002, "Ultralight Porous Metals: From Fundamentals to Applications," Acta Mech. Sin., **18**(5), pp. 457–479.
[18] Giuliano, M. R., Prasad, A. K., and Advani, S. G., 2012, "Experimental Study of an Air-Cooled Thermal Management System for High Capacity Lithium-Titanate Batteries," J. Power Sources, **216**, pp. 345–352.
[19] Mavridou, S., Mavropoulos, G. C., Bouris, D., Hountalas, D. T., and Bergeles, G., 2010, "Comparative Design Study of a Diesel Exhaust Gas Heat Exchanger for Truck Applications With Conventional and State of the Art Heat Transfer Enhancements," Appl. Therm. Eng., **30**(8–9), pp. 935–947.
[20] Jeng, T. M., and Tzeng, S. C., 2005, "Numerical Study of Confined Slot Jet Impinging on Porous Metallic Foam Heat Sink," Int. J. Heat Mass Transfer, **48**(23–24), pp. 4685–4694.
[21] Ejlali, A., Ejlali, A., Hooman, K., and Gurgenci, H., 2009, "Application of High Porosity Metal Foams as Air-Cooled Heat Exchangers to High Heat Load Removal Systems," Int. Commun. Heat Mass Transfer, **36**(7), pp. 674–679.
[22] Marafie, A., Khanafer, K., Al-Azmi, B., and Vafai, K., 2008, "Non-Darcian Effects on the Mixed Convection Heat Transfer in a Metallic Porous Block With a Confined Slot Jet," Numer. Heat Transfer, Part A, **54**(7), pp. 665–685.
[23] Kuang, J. J., Kim, T., Xu, M. L., and Lu, T. J., 2012, "Ultralightweight Compact Heat Sinks With Metal Foams Under Axial Fan Flow Impingement," Heat Transfer Eng., **33**(7), pp. 642–650.
[24] Shih, W. H., Chiu, W. C., and Hsieh, W. H., 2006, "Height Effect on Heat-Transfer Characteristics of Aluminum-Foam Heat Sinks," ASME J. Heat Transfer, **128**(6), pp. 530–537.
[25] Rallabandi, A. P., Rhee, D. H., Gao, Z. H., and Han, J. C., 2010, "Heat Transfer Enhancement in Rectangular Channels With Axial Ribs or Porous Foam Under Through Flow and Impinging Jet Conditions," Int. J. Heat Mass Transfer, **53**(21–22), pp. 4663–4671.
[26] Bhattacharya, A., and Mahajan, R. L., 2002, "Finned Metal Foam Heat Sinks for Electronics Cooling in Forced Convection," ASME J. Electron. Packag., **124**(3), pp. 155–163.
[27] Bhattacharya, A., and Mahajan, R. L., 2006, "Metal Foam and Finned Metal Foam Heat Sinks for Electronics Cooling in Buoyancy-Induced Convection," ASME J. Electron. Packag., **128**(3), pp. 259–266.
[28] DeGroot, C. T., Straatman, A. G., and Betchen, L. J., 2009, "Modeling Forced Convection in Finned Metal Foam Heat Sinks," ASME J. Electron. Packag., **131**(2), p. 021001.
[29] Krishnan, S., Hernon, T. D., Hodes, M., Mullins, J., and Lyons, A. M., 2012, "Design of Complex Structured Monolithic Heat Sinks for Enhanced Air Cooling," IEEE Trans. Compon. Packag. Manuf. Technol., **2**(2), pp. 266–277.
[30] Feng, S. S., Kuang, J. J., Wen, T., Lu, T. J., and Ichimiya, K., 2014, "An Experimental and Numerical Study of Finned Metal Foam Heat Sinks Under Impinging Air Jet Cooling," Int. J. Heat Mass Transfer, **77**, pp. 1063–1074.
[31] Calmidi, V. V., and Mahajan, R. L., 2000, "Forced Convection in High Porosity Metal Foams," ASME J. Heat Transfer, **122**(3), pp. 557–565.
[32] Vafai, K., and Tien, C. L., 1981, "Boundary and Inertia Effects on Flow and Heat-Transfer in Porous Media," Int. J. Heat Mass Transfer, **24**(2), pp. 195–203.
[33] Patankar, S. V., 1980, *Numerical Heat Transfer and Fluid Flow*, McGraw-Hill, New York, Sect. 5.5-2, p. 102.
[34] Eckert, E. R. G., and Drake, R. M., 1980, *Analysis of Heat and Mass Transfer*, McGraw-Hill, New York.
[35] Feng, S. S., Kim, T., and Lu, T. J., 2013, "Numerical Investigation of Forced Convection in Pin/Plate-Fin Heat Sinks Heated by Impinging Jet Using Porous Medium Approach," Int. J. Numer. Methods Heat Fluid Flow, **23**(1), pp. 88–107.
[36] Feng, S. S., Kim, T., and Lu, T. J., 2010, "A Semi-Empirical Heat Transfer Model for Forced Convection in Pin-Fin Heat Sinks Subjected to Non-Uniform Heating," ASME J. Heat Transfer, **132**(12), p. 121702.
[37] Jeng, T. M., and Tzeng, S. C., 2005, "A Semi-Empirical Model for Estimating Permeability and Inertial Coefficient of Pin-Fin Heat Sinks," Int. J. Heat Mass Transfer, **48**(15), pp. 3140–3150.
[38] Mills, A. F., 1995, *Basic Heat and Mass Transfer*, Richard D. Irwin, Inc., Chicago.
[39] Zhao, C. Y., and Lu, T. J., 2002, "Analysis of Microchannel Heat Sinks for Electronics Cooling," Int. J. Heat Mass Transfer, **45**(24), pp. 4857–4869.